# Title: Cenozoic evolution of deep ocean temperature from clumped isotope thermometry

**Authors:** A.N. Meckler[1*], P.F. Sexton[2], A.M. Piasecki[1†], T.J. Leutert[1], J. Marquardt[1], M. Ziegler[3], T. Agterhuis[3], L.J. Lourens[3], J.W.B. Rae[4], J. Barnet[4], A. Tripati[5], S.M. Bernasconi[6].

**Affiliations:**

[1]Bjerknes Centre for Climate Research and Department of Earth Science, University of Bergen; Bergen, Norway.

[2]School of Environment, Earth and Ecosystem Sciences, The Open University; Milton Keynes, UK.

[3]Faculty of Geosciences, Utrecht University, Utrecht, The Netherlands.

[4]School of Earth and Environmental Sciences, University of St. Andrews, St. Andrews, UK.

[5]Department of Earth, Planetary, and Space Science, Department of Atmospheric and Oceanic Science, Institute of the Environment and Sustainability, American Indian Studies Center, Center for Diverse Leadership in Science, University of California Los Angeles; Los Angeles, USA.

[6]Department of Earth Science, ETH Zürich; Zürich, Switzerland.

*Corresponding author. Email: nele.meckler@uib.no.

†Present address: CIRES, University of Colorado, Boulder, USA.

**Abstract:** Characterizing past climate states is crucial for understanding future consequences of ongoing greenhouse gas emissions. Here we revisit the benchmark oxygen isotope time series for deep ocean temperature across the last 65 million years using clumped isotope thermometry. Our Atlantic Ocean deep ocean temperatures are overall much warmer compared to earlier oxygen isotope-based estimates, highlighting the likely influence of changes in deep ocean pH and/or seawater oxygen isotope composition on classical $\delta^{18}O$ records of the Cenozoic. In addition, our data reveal previously unrecognized large swings in deep ocean temperature during early Eocene acute greenhouse warmth. Our results call for a reassessment of the Cenozoic history of ocean temperatures to achieve a more accurate understanding of the nature of climatic responses to tectonic events and variable greenhouse forcing.

**One Sentence Summary:** Past greenhouse climates were associated with warmer and more variable deep ocean temperatures than previously thought.

**Main Text:**

Through the Cenozoic era (the last 65 million years), Earth experienced a large range of climate states (Westerhold et al., 2020; Zachos et al., 2001), moving from greenhouse climates with high levels of atmospheric carbon dioxide ($CO_2$) and minimal ice on land, to an icehouse world with large-scale, bipolar glaciation. Reconstructions of past temperatures offer unique insights into the response of the climate system to varying levels of $CO_2$ as well as tectonically forced changes in ocean circulation. These reconstructions additionally serve as crucial benchmarks for assessing the performance of climate models (Lunt et al., 2021). To obtain globally representative temperature estimates on million-year timescales, deep ocean temperature is commonly used (e.g., Burke et al., 2018; Inglis et al., 2020), given that the deep ocean constitutes an extremely large and comparatively stable heat reservoir.

The key approach to reconstruct deep ocean temperatures, especially through the early Cenozoic, has been analyses of the oxygen isotopic composition of shells of benthic foraminifera ($\delta^{18}O_b$) from deep ocean sediments. $\delta^{18}O_b$ reflects deep ocean temperature, but also seawater isotopic composition ($\delta^{18}O_{sw}$) at the time of shell formation. The canonical view has been that, prior to Antarctica being continually glaciated, $\delta^{18}O_{sw}$ had an assumed "ice-free" value of -0.9 to -1.2 ‰ (Cramer et al., 2011; Zachos et al., 2001), and that temperature was the single most important influence on $\delta^{18}O_b$. Paleocene and early to middle Eocene temperatures are therefore typically calculated directly from $\delta^{18}O_b$ using established temperature calibrations (e.g., Marchitto et al.,

2014). This approach has yielded deep ocean temperatures of up to 12 °C (Zachos et al., 2001) to 14 °C (Cramer et al., 2011) during the warmest part of the Cenozoic, the early Eocene climatic optimum (EECO, 52-49 Ma). Yet the long-standing assumptions made as part of this established approach are largely uncorroborated (Cramer et al., 2011; Hollis et al., 2019). Seawater $\delta^{18}O$ indeed reflects continental storage of ice, but also of groundwater, and can in addition be influenced by changes in salinity, as well as long-term changes in interactions between seawater and oceanic crust. Furthermore, non-thermal, physiological influences on $\delta^{18}O_b$ of benthic foraminifera are not well understood (Marchitto et al., 2014), but are evident from $\delta^{18}O_b$ offsets between different species (e.g., Katz et al., 2003).

Additional proxy constraints have previously been sought from the Mg/Ca ratio of benthic foraminifera (e.g., Lear et al., 2000; Tripati et al., 2005), a temperature proxy that is independent of $\delta^{18}O_{sw}$. However, like $\delta^{18}O_b$, the Mg/Ca proxy suffers from non-thermal influences such as changes in seawater Mg/Ca ratio and pH (*13*), and physiological effects necessitating species-specific calibrations (Hollis et al., 2019). Given these potential confounding influences on $\delta^{18}O_b$, the Cenozoic evolution of deep ocean temperature remains highly uncertain.

Here we report the first Cenozoic record of deep ocean temperature based on carbonate clumped isotope ($\Delta_{47}$) thermometry. The clumped isotope method takes advantage of the temperature dependence of isotopic ordering within molecules (Eiler, 2007) and has the benefit that it does not require knowledge about seawater composition and is not measurably affected by physiological factors during the formation of foraminifera shells (supplementary methods). Our record is predominantly from sites with exceptional foraminifera preservation in the North

Atlantic, a region of major influence on global ocean circulation and climate. The reported clumped isotope temperatures each combine 13-45 replicate analyses of different foraminifera species, with species- or genus-specific $\delta^{18}O_b$ and $\delta^{13}C$ obtained from the same measurements. The $\Delta_{47}$ temperatures show many similarities, but also striking differences, compared to previous reconstructions of deep ocean temperatures based on $\delta^{18}O_b$ (Fig. 1A, Fig. S6). We observe the same overall trend across the Cenozoic, attesting to the fact that the large-scale features of the canonical $\delta^{18}O_b$ dataset do indeed reflect overall cooling through the Cenozoic. This confirmation is especially important in light of a recent, controversial suggestion that attributes the Cenozoic trend of increasing $\delta^{18}O_b$ to post-depositional alteration during burial (Bernard et al., 2017; Evans et al., 2018). However, $\Delta_{47}$ temperatures are considerably warmer than previous multi-proxy estimates during most of the Cenozoic (Fig. 1A), with deviations of 3-5 °C in the middle Oligocene and late Eocene and up to 6-8 °C in some late Paleocene and early Eocene intervals. Our $\Delta_{47}$ data also reveal large temperature changes in the early Eocene (48-56 Ma) not apparent in the $\delta^{18}O_b$-based record.

Most of our $\Delta_{47}$ data are from the North Atlantic, a region that is seldom represented in Cenozoic climate records. The divergences from $\delta^{18}O_b$-based reconstructions could hence reflect regional differences. However, our North Atlantic $\delta^{18}O_b$ and $\delta^{13}C$ data obtained alongside the $\Delta_{47}$ measurements show generally close agreement with equivalent global records (Fig. 1B, C, supplement). We furthermore find excellent agreement of our $\Delta_{47}$ temperatures with previous and new $\Delta_{47}$-based temperature estimates from other locations. Our middle Miocene temperature estimates agree with results from the Indian and Southern Ocean at that time (Fig. 1A, pink triangles) (Leutert et al., 2021; Modestou et al., 2020). For the Eocene, North Atlantic

temperatures are similar to those in the tropical and South Atlantic Ocean (Fig. 1A, yellow circle and pink stars) (Agterhuis et al., in revision; Leutert et al., 2019), including the South Atlantic location that represents the backbone for the early Cenozoic global $\delta^{18}O_b$ record. While further validation of the globally representative nature of North Atlantic temperatures awaits detailed $\Delta_{47}$ records from multiple sites, the available data point to our $\Delta_{47}$ temperatures being representative of significant parts of the global ocean.

The consistency in $\Delta_{47}$ temperatures between different locations furthermore argues against a strong influence of post-depositional alteration of the $\Delta_{47}$ signal that would likely be site-specific. Preservation of foraminifera at the North Atlantic sites is typically good to excellent (Fig. S2) and thus superior to many other deep ocean locations from which $\delta^{18}O$ data have been generated, and we observe no relationship between foraminifer preservation state and $\Delta_{47}$ temperature (Fig. S1, S2). Our Pleistocene $\Delta_{47}$-based temperatures of 0.0 - 3.4 °C (Fig. S4) are in agreement with observed present-day (~3°C) and reconstructed glacial temperatures (-1 °C (Thiagarajan et al., 2014)), further attesting to the reliability of the clumped isotope temperatures.

**Fig. 1. Clumped isotope-based reconstruction of deep ocean temperatures in comparison with classical foraminifera isotope records.** See also Fig. S4 for close-up for early and late Cenozoic intervals. (**A**) $\Delta_{47}$ temperatures from the North Atlantic (grey symbols), in comparison with estimates from other sites (purple shaded symbols, see inset map) in the Indian Ocean (middle Miocene; (Modestou et al., 2020)), equatorial and South Atlantic (this study, Agterhuis et al., in revision; Leutert et al., 2019), and Atlantic sector of the Southern Ocean (Agterhuis et al., in revision). The early Eocene data from (Agterhuis et al., in revision) span a time interval of ~200 kyr and were combined into one data point for each location. Error bars for $\Delta_{47}$ temperatures are 68% (solid lines) and 95% (stippled lines) confidence intervals. For the North Atlantic, darkness of shading reflects robustness based on degree of replication (from 13 to >35 replicates). The other data points are based on 30 to >200 measurements (see Table S1), reflected

in the size of the error bars. The grey stippled line is a LOESS fit through the North Atlantic data with a Monte Carlo-based 95% confidence interval (see supplementary information). The red line is a previous estimate of deep ocean temperature based on $\delta^{18}O_b$ and sea level reconstructions (Cramer et al., 2011). (**B**) CENOGRID $\delta^{18}O_b$ record (Westerhold et al., 2020) and $\delta^{18}O_b$ results from species of the genus *Cibicidoides* (circles) and *Nuttalides* (crosses) from the clumped isotope analyses, corrected for interspecies offsets (*Cibicidoides:* +0.64 ‰; *Nuttalides:* +0.4 ‰). (**C**) CENOGRID $\delta^{13}C$ record (Westerhold et al., 2020) with results from *Cibicidoides* and *Nuttalides* species from the clumped isotope analyses. Note that the global CENOGRID record also includes corrections for offsets between sites/ocean basins, which we do not apply to our data. Typical offsets in $\delta^{18}O_b$ between Atlantic and Pacific sites (the latter interpreted as equivalent to global) are on the order of -0.2 to -0.3 ‰ for the Eocene to Oligocene (Westerhold et al., 2020), compared to 0 to -0.5 ‰ offsets in our *Nuttalides* data. Inset map shows site locations on a paleogeographic reconstruction for ~50 Ma (www.odsn.de/odsn/services/paleomap/paleomap.html).

Compared to previous estimates based on $\delta^{18}O_b$ (Fig. 1A, S6), the overall warmer $\Delta_{47}$-based deep ocean temperatures are more consistent with reconstructed warm high-latitude surface ocean temperatures (e.g., Hollis et al., 2019), thought to reflect the main source regions of deep water for much of the Cenozoic. The deviation of $\Delta_{47}$-based from $\delta^{18}O_b$-based temperatures could imply that deep ocean $\delta^{18}O_{sw}$ was higher than previously thought (Fig. 2D, blue symbols versus grey line), for example because of intensified crustal interaction with seawater owing to faster seafloor spreading, or from substantial continental storage of $^{16}O$ in ice sheets or as groundwater. $\delta^{18}O_{sw}$ values, calculated from $\Delta_{47}$ temperatures, regularly approach 1 ‰ in the North Atlantic and the other locations (Fig. 2D; (Modestou et al., 2020)). If wholly explained by continental ice sheets, this would imply that ice sheets reached sizes similar to the Last Glacial Maximum, which seems implausible. Nevertheless, uncertainties in the size of Cenozoic ice sheets translate into uncertainties in $\delta^{18}O_{sw}$ and thus could contribute to the discrepancies in temperature estimates from $\Delta_{47}$ and $\delta^{18}O_b$. Enhanced storage of $^{16}O$-enriched groundwater could also have increased $\delta^{18}O_{sw}$ and has been proposed for the Cretaceous greenhouse (e.g., Wendler et al.,

2016) but the magnitude of this effect is uncertain (Davies et al., 2020). Parts of the ocean interior could at times have been filled with more saline $^{18}O$-enriched water. Overall, any of these factors or a combination of them could have contributed to elevating $\delta^{18}O_{sw}$ during much of the Cenozoic, but their potential influence remains unclear.

Instead of an underestimation of $\delta^{18}O_{sw}$, another possibility is that the incorporation of the $\delta^{18}O$ signal in foraminifera could be affected by non-thermal influences, such as ocean pH. Based on new and published boron isotope data from benthic foraminifera, we reconstruct a pH increase of ~0.6 pH units in the deep ocean over the course of the Cenozoic (Fig. 2C), corresponding to a substantial decrease in atmospheric $CO_2$ concentration (Fig. 2B; (Anagnostou et al., 2020; Rae et al., 2021)). While evidence for a pH effect on benthic foraminifer $\delta^{18}O_b$ is currently unresolved (Marchitto et al., 2014), the theoretical effect of 1.42 ‰ per pH unit (Zeebe, 2001), as observed in planktic foraminifera (Spero et al., 1997), would bias early Cenozoic $\delta^{18}O_b$-based temperatures by ~4 °C. A pH influence on $\Delta_{47}$, if present, would bias those temperatures in the same direction, but the effect should be approximately four times smaller than for $\delta^{18}O$-derived temperatures (Guo, 2020; Tripati et al., 2015) and has so far not been observed in the typical oceanic pH range (Tang et al., 2014). Although we cannot conclusively demonstrate a pH effect on benthic $\delta^{18}O_b$, it is intriguing that correcting $\delta^{18}O_b$ for the overall Cenozoic trend in deep ocean pH, assuming the same effect as in planktic species (Fig. 2D, light green symbols), brings calculated $\delta^{18}O_{sw}$ into closer agreement with previous estimates based on sea level reconstructions (Cramer et al., 2011): average $\delta^{18}O_{sw}$ for >45 Ma becomes -0.72 ‰ versus 0.04 ‰ without pH correction; Fig 2D). This improved agreement points to a pH effect being a likely explanation for the long-term disagreement between $\delta^{18}O_b$- and $\Delta_{47}$-based temperatures.

Renewed efforts should focus on investigating pH effects on $\delta^{18}O$ and $\Delta_{47}$ in benthic foraminifera to test this hypothesis.

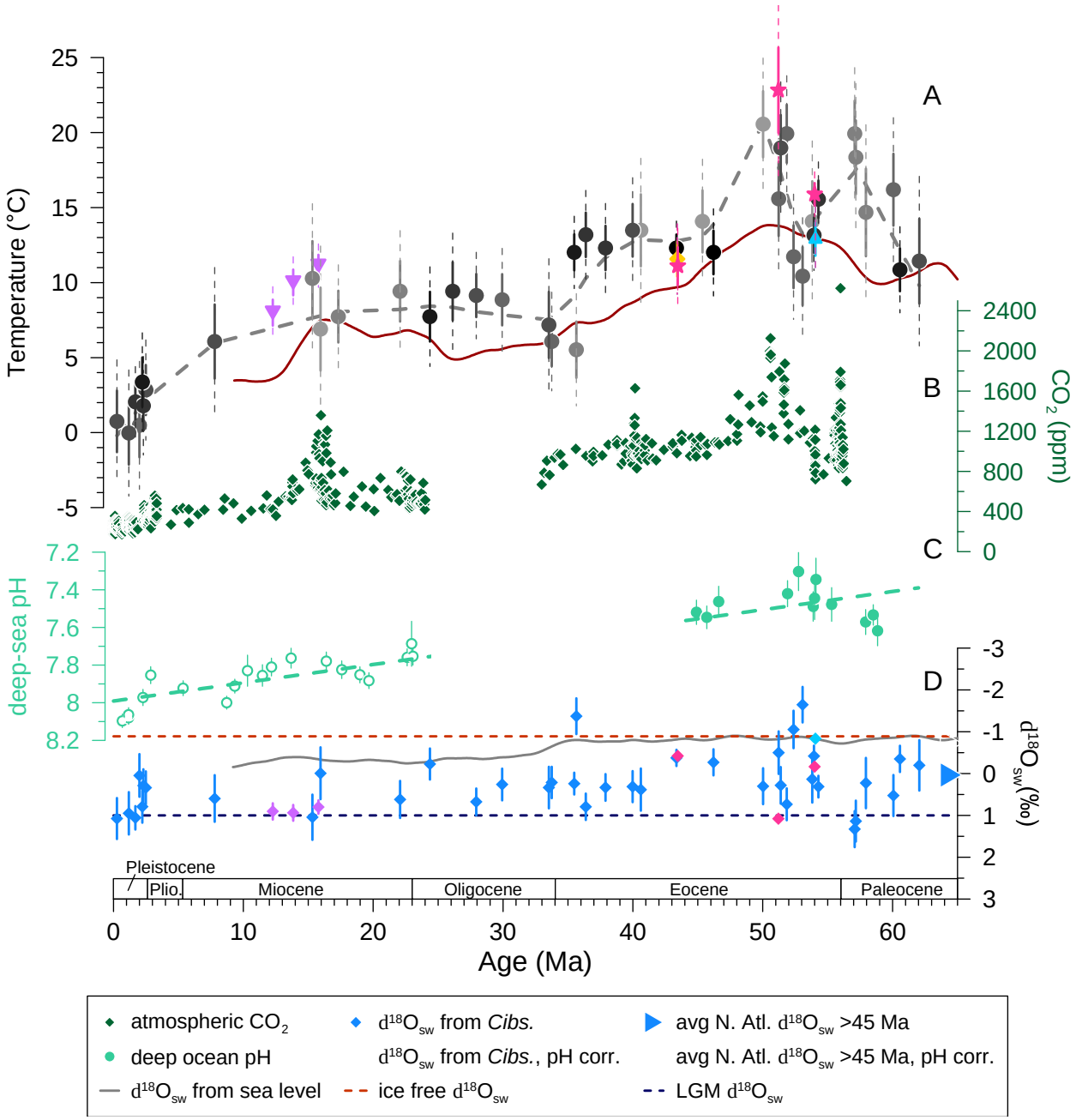


**Fig. 2. Cenozoic evolution of seawater isotopic composition and comparison with changes in the carbon cycle.** (**A**) $\Delta_{47}$ temperatures as in Fig. 1with (**B**) atmospheric $CO_2$ concentration from boron isotopes in planktic foraminifera (Rae et al., 2021) with 1 SD uncertainties, and (**C**) reconstructed deep ocean pH from boron isotopes in benthic foraminifera ((Greenop et al., 2017),

open symbols; *this study*, closed symbols) with linear regression; error bars show the influence of uncertainties in $\delta^{11}B$ and temperature at 2 SD and the shaded area reflects the influence of $\delta^{11}B_{SW}$ ±0.5 ‰ (see methods). (**D**) Calculated $\delta^{18}O_{sw}$ (against the SMOW standard; blue/purple symbols with 68% and 95% confidence intervals) compared to suggested "ice-free" $\delta^{18}O_{sw}$ of -0.9 ‰ (red stippled line; (Cramer et al., 2011)), $\delta^{18}O_{sw}$ of Pleistocene glacial periods of 1 ‰ (dark blue stippled line), and $\delta^{18}O_{sw}$ reconstructed from sea level estimates and the estimated ice-free $\delta^{18}O_{sw}$ ((Cramer et al., 2011); grey line). Blue data points are from the North Atlantic and other colors reflect other sites (see Fig. 1). Light green and other faded color symbols are $\delta^{18}O_{sw}$ estimates after correcting $\delta^{18}O_b$ for the long-term increase in deep ocean pH (panel C) and assuming a sensitivity of 1.42 ‰ per pH unit (Zeebe, 2001). While this first-order correction does not eliminate the variability in $\delta^{18}O_{sw}$, it brings the values on average in closer agreement with the estimated ice-free $\delta^{18}O_{sw}$ for the early part of the record. Arrows on the right show the average $\delta^{18}O_{sw}$ values for >45 Ma before and after (light green) pH correction.

Superimposed on the general trend in $\Delta_{47}$ temperatures, some intervals like the late Eocene and especially the late Paleocene-early Eocene stand out with substantial temperature variability that is not apparent to the same extent in our $\delta^{18}O_b$ data or the global $\delta^{18}O_b$ record (Fig 1A, B). While the late Eocene variability currently hinges on one anomalously cold data point at ~35.6 Ma, which could correspond to a previously reported late Eocene cooling event in the North Atlantic and elsewhere (Sliwinska et al., 2019), the temperature variations in the late Paleocene-early Eocene appear to be of longer duration and are better constrained. There we observe multi-million-year-long temperature swings with a first warming of ~4 °C between 58 and 57 Ma, followed by cooling of ~4 °C between 57 and 54 Ma, further ~3 °C cooling between 54 and 53 Ma, and a second, major warming of 7-8 °C at 52 Ma (Figs. 1, S4). Distinct cold spells around 55 Ma have previously been reported for the North Atlantic region (Vickers et al. ref), and the $\Delta_{47}$ temperatures from Agterhuis et al. show that these extended to the deep South Atlantic (Fig. 1A, pick star and blue triangle).

The early Eocene is characterized by strong orbital-scale climate variability depicted by variations in $\delta^{18}O_b$ (Westerhold et al., 2020) of up to 1 ‰ (4-5 °C using traditional assumptions), which, in principle, could have been aliased by our lower resolution $\Delta_{47}$ sampling. However, the $\delta^{18}O_b$ data we obtained with the $\Delta_{47}$ measurements do not show anything resembling the scale of variability suggested by $\Delta_{47}$. This discrepancy between $\Delta_{47}$ and $\delta^{18}O_b$ is reflected in substantial temporal variability in calculated $\delta^{18}O_{sw}$. Given the large variations in atmospheric $CO_2$ of up to 1000 ppm during the early Eocene (Fig. 2B; (Anagnostou et al., 2020)), it is likely that deep ocean pH changed more frequently and substantially over this interval than our $\delta^{11}B$ record shows. Such changes in pH would likely dampen any high amplitude temperature variance recorded in $\delta^{18}O_b$. However, pH-induced dampening can likely not explain the full scale of the difference between $\delta^{18}O_b$ and $\Delta_{47}$. Changes in crustal exchange and ice volume are similarly unlikely causes for these comparatively rapid fluctuations in $\delta^{18}O_{sw}$ under peak greenhouse warmth. Instead, the Eocene $\delta^{18}O_{sw}$ signal is best explained by changes in deep ocean salinity, with colder temperatures between 54 and 52 Ma accompanied by fresher deep water (low $\delta^{18}O_{sw}$), and peak temperatures at 52-49 Ma and 57-60 Ma associated with high $\delta^{18}O_{sw}$ values implying saltier deep water.

Tectonic activity and seafloor spreading in the northern North Atlantic intensified at ~57 Ma, diminished at 52 Ma, while intensifying again at 48 Ma (Gaina and Jakob, 2019), which may have modified Arctic-North Atlantic oceanic connections, with potentially major effects on Atlantic ocean circulation. The transitions to colder and fresher deep water sometime between 57 and 54 Ma and back to warm salty deep water at 52 Ma also coincide with a marked increase and subsequent decrease in foraminifera $\delta^{13}C$ (Fig. 1C) that may reflect changes in ocean circulation.

The temperature swings were also accompanied by inferred shifts from low latitude warm, oxygen-poor intermediate and deep water mass sources to high latitude, colder, oxygen-rich sources based on nitrogen and sulfur isotope records ((Kast et al., 2019; Rennie et al., 2018); Fig. S7). These latter biogeochemical tracers infer step-changes rather than the transient temperature swings revealed by $\Delta_{47}$, possibly because they reflect intermediate rather than deep water masses, and/or changes in other ocean basins that might differ from those in the deep Atlantic. Regardless, multiple lines of evidence indicate large-scale reorganizations in water mass structure in the Atlantic, and possibly the global ocean, during the early Eocene.

The observed switches between warm and cold deep-water masses with inferred accompanying changes in salinity imply the need to reassess the interpretation of $\delta^{18}O_b$ records. Temperature and salinity are the key determinants of seawater density; given that both influence $\delta^{18}O_b$, $\delta^{18}O_b$ has previously been invoked as an integrated proxy for seawater density (*34*), rather than for either of the underlying parameters in isolation. Calculating density from $\delta^{18}O_b$ is, however, complicated by large variations in the $\delta^{18}O_{sw}$ – salinity relationship (*34*). Nonetheless, at any given depth in the deep ocean, density is likely more stable than temperature or salinity alone, which could explain why $\delta^{18}O_b$ does not record the temperature swings we observe with $\Delta_{47}$. During the early Eocene, latitudinal temperature gradients were reduced (e.g., Hollis et al., 2019), salinity gradients were enhanced owing to a stronger hydrological cycle (Zhu et al., 2020), and shallow tropical seas were more widespread. Under these conditions, saline water masses originating at low to mid latitudes could have been more prevalent at times. Density differences may have been small enough to allow for coexistence of, and switches between, water masses of very different temperatures and/or salinities, as has been proposed for the

Paleocene-Eocene Thermal Maximum (e.g., Tripati and Elderfield, 2005). On timescales shorter than possible variations in the global ocean water isotope budget, the overall isotope budget must stay balanced, calling for freshening in other parts of the ocean during times when the deep Atlantic ocean was filled with saltier water. Our data suggest that the early Eocene greenhouse was characterized by a more dynamic deep-water mass structure than previously appreciated.

The strong temperature variations we observe in the deep Atlantic during the early Eocene are not reflected in the contemporaneous sea surface temperature records available (Fig. S5). Although there is a geographic scarcity of records, and the potential for large geographic differences in sea surface temperatures (Douglas et al., 2014), at face value this discrepancy between deep ocean and sea surface temperatures lends support to changes in the structure of deep-water masses as the main cause of the strong deep ocean temperature variations, as opposed to wholesale swings in global mean temperature. Yet the pronounced warming at 52 Ma intriguingly coincides with a marked increase in reconstructed atmospheric $CO_2$ ((Anagnostou et al., 2020; Rae et al., 2021); Fig. 2B), calling for increased focus on detailed temperature reconstructions from both the surface and deep ocean across this significant time interval.

While our data confirm the first-order Cenozoic cooling trend in the deep ocean, they also reveal that our canonical views on $\delta^{18}$O-ice volume-temperature relationships do not hold true through the Cenozoic, implying that $\delta^{18}O_b$ should not be used as a direct temperature proxy without further research. If our warmer deep ocean temperatures turn out to be representative for a large fraction of the global ocean, it would lead to a higher climate sensitivity to atmospheric $CO_2$ during Cenozoic greenhouse climates (Agterhuis et al., in revision; Anagnostou et al., 2020)

compared to previous estimates (Inglis et al., 2020). Our finding of major variations in deep ocean temperature during the early Eocene that are not apparent in $\delta^{18}O_b$ points to an interpretation of $\delta^{18}O_b$ in terms of seawater density during times of minimal continental ice. Together, these constraints on deep ocean properties emerging from the application of clumped isotope thermometry offer the opportunity to investigate not only overall greenhouse climate states but also climate (in)stability under such warmer-than-modern boundary conditions.

**Acknowledgments:** We acknowledge technical help during sample preparation and clumped isotope analyses by N. Irvalı, R. Tapia, L. Griem, J. Donn Holl, L. Al-Saadi, V. Taylor, E. Alagoz, and E. Vinje Galaasen. A. Fernandez Bremer is acknowledged for sharing his Matlab code for error propagation. For the analyses at Utrecht University, I.J. Kocken is acknowledged for processing the clumped isotope data archive with his R script, A. Roozendaal is thanked for sample preparation, and A. E. van Dijk provided technical support in the lab. M. Kaminski and E. Littley are thanked for assistance with boron isotope analyses. This research used samples and data from the International Ocean Discovery Program (IODP) the Ocean Drilling Program (ODP). The manuscript benefited from the constructive comments of the reviewers.

**Funding:**

Swiss National Science Foundation MHV fellowship (ANM)
European Research Council Starting Grant Nr. 638467 (ANM)
Trond Mohn Foundation Starting Grant Nr. BFS2015REK01 (ANM)
Norwegian Research Council Infrastructure Grant Nr. 245907 (ANM)
Natural Environment Research Council (NERC) grant nr. NE/P019331/1 (PFS)
European Research Council Starting Grant Nr. 805246 (JWBR)
Dutch Research Council (NWO) VIDI project 016.161.365 (MZ)
Netherlands Earth System Science Centre (NESSC) (LJL)

**Author contributions:**

Initiation: ANM, AT
Conceptualization: ANM, PFS, AT, MZ, SMB

Methodology: ANM, MZ, SMB
Resources: PFS, JWBR, LJL
Investigation: ANM, PFS, AMP, TJL, JM, TA, MZ, LJL, JB, JWBR
Funding acquisition: ANM, PFS, MZ, LJL, JWBR, AT, SMB
Writing – original draft: ANM, PFS, MZ, JWBR
Writing – review & editing: ANM, PFS, TJL, JM, MZ, TA, LJL, JWBR, JB, AT, SMB

**Competing interests:** The authors declare that they have no competing interests.

**Data and materials availability:** Data will be available from the Earthchem (replicate-level $\Delta_{47}$ data with standard data and detailed data processing information) and Pangaea (sample-average $\Delta_{47}$ temperatures, $\delta^{18}O_b$ and $\delta^{18}O_{sw}$) databases.

**Supplementary Materials**

Materials and Methods

References (*38-71*)

Figs. S1 to S7

Tables S1 to S2

Data S1 to S2

**Materials and Methods**

Material

1. Newfoundland Margin

Large individual samples, for the most part core catchers, were taken from four different International Ocean Discovery Program (IODP) sites recovered by Expedition 342 on the Newfoundland margin in the North Atlantic (1406, 1407, 1409, and 1410; Table S1, Fig. S1), together covering the entire Cenozoic era (Scientists, 2012). Age models for all Sites are based on detailed integrated bio-magneto-stratigraphies (Scientists, 2012), updated to the CENOGRID timescale (Westerhold et al., 2020). Other supporting datasets that we show in Figures 1 and 2

(atmospheric $CO_2$ and previous estimates of deep ocean temperature and $\delta^{18}O_{sw}$) are plotted on their published age models; minor resulting differences in age models are not relevant on the timescales investigated here.

**Table S1**. IODP Sites from Newfoundland margin studied, with their respective water depths below sea level at present (Scientists, 2012) and at 50 Ma (Tucholke and Vogt, 1979).

| Site | Present location | Water depth (m) present | Water depth (m) 50 Ma |
|---|---|---|---|
| U1407 | 41°25.5'N, 49°48.8'W | 3074 | 2600 |
| U1410 | 41°19.7'N, 49°10.2'W | 3387 | 2950 |
| U1409 | 41°17.7'N, 49°14.0°W | 3500 | 3050 |
| U1406 | 40°21.0'N, 51°39.0'W | 3813 | 3300 |

For each sample, benthic foraminifera were picked from size fractions >150 µm. A large variety of foraminifer species were used for analysis in order to achieve the necessary level of replication (Data S2), whereby aliquots for measurements were separated on the species or at least genus level where possible. Aliquots were cleaned by carefully opening foraminifera tests, followed by several iterations of ultrasonication using both deionized water and methanol, with subsequent rinses with deionized water and oven-drying at 50°C.

Scanning electron microscope images were obtained from a random selection of cleaned sample aliquots distributed over the whole study interval (Fig. S2).

2. Walvis Ridge

For the Early Eocene, one additional clumped isotope temperature was obtained from Site 1263 (paleo-water depth ~1500 m) on the Walvis Ridge in the South Atlantic as an average of analyses from multiple individual samples spanning ~400 kyr (from 51.3 to 50.9 Ma). Foraminifer species *Nuttalides truempyi* and *Oridorsalis umbonatus* from the > 212 µm size fraction were cleaned and analyzed at Utrecht University.

Methods

1. Clumped isotope thermometry

Clumped isotope thermometry takes advantage of the temperature dependence of isotopic ordering within molecules, with double substitution by heavy isotopes (e.g., $^{18}O$ and $^{13}C$ in carbonates) increasing with decreasing formation temperature (Eiler, 2007). The excess abundance of such double substitution in carbonates compared to random ordering ($\Delta_{47}$) is independent of the

composition of the source water. The signal furthermore does not exhibit biological effects in foraminifera (Grauel et al., 2013; Meinicke et al., 2020; Peral et al., 2018; Piasecki et al., 2019; Tripati et al., 2010), appears to not be measurably affected by seawater pH within the range typical for the ocean (Tang et al., 2014; Tripati et al., 2015), and is largely robust to diagenetic overprinting in benthic foraminifera from typical ocean settings (Leutert et al., 2019), if burial depth was sufficiently shallow (Stolper et al., 2018). Using carbonate-based standardization (Bernasconi et al., 2018), calibrations can be reproduced in different laboratories, and foraminifera-based calibrations are indistinguishable from inorganically precipitated calcite (Meinicke et al., 2020; Peral et al., 2018; Tripati et al., 2010). The comparatively large analytical uncertainty due to a small signal-to-noise ratio can be mitigated by extensive replication, where sample availability permits.

Clumped isotope measurements were performed between 2015 and 2020 on four different mass spectrometers in Bergen, Zürich, and Utrecht, all consisting of Thermo Fisher Scientific MAT253 or MAT253Plus instruments coupled to Thermo Fisher Scientific Kiel IV carbonate preparation devices. Most of the analyses (N = 936) were performed on two different mass spectrometers in Bergen, with the exception of some North Atlantic sample aliquots measured in Zürich (N = 43), and early Eocene samples from Walvis Ridge analyzed in Utrecht (N = 30). The analytical approach was similar to that described by (Meckler et al., 2014) and updated for the Bergen analyses as described by (Piasecki et al., 2019) and (Meinicke et al., 2020). The methodological details for the Utrecht lab are described in (Agterhuis et al., in revision). In the Kiel device, sample aliquots are individually reacted with phosphoric acid at 70°C, and the sample gas is cryogenically separated from water and other trace gases. All Kiel devices were equipped with additional custom-built traps for organic contaminants (Porapak Q columns, held at -20°C; -45°C in the Utrecht lab) and sulfide components (Ag wool). All measurements were conducted in microvolume mode, and in the case of the Bergen and Utrecht instruments, the long-integration-dual-inlet method (LIDI; (Hu et al., 2014)) was used. Masses 44-49 were monitored, and masses 44-47 were used for calculating $\delta^{13}C$, $\delta^{18}O$, and $\Delta_{47}$. The raw data were corrected for pressure baseline effects based on daily peak scans (Meckler et al., 2014) and further corrections for $\Delta_{47}$ scale compression and transfer to the I-CDES scale (Bernasconi et al., 2021) were made using carbonate standards ETH 1-3. The accepted values of these standards were derived by multiple laboratories (Bernasconi et al., 2021) and reported for an acid digestion temperature of 90 °C. Our $\Delta_{47\ (I\text{-}CDES)}$ results therefore also reflect an acid digestion temperature 90 °C (but note that by using carbonate standards, no acid fractionation factor needs to be applied). Standard aliquots were measured in roughly equal numbers as sample aliquots. In most cases, a moving window approach was used to base corrections on standard data from several adjacent days, with the number of standard measurements used for corrections depending on instrument stability. For the measurements performed in Bergen, data corrections were done with the Easotope software (John and Bowen, 2016). All replicate-level data are archived in the Earthchem database (doi: *to be inserted when available*), including information regarding standard correction procedures.

Sample-averaged data are reported as supplementary Data S1 and archived in the Pangaea database (doi: *to be inserted when available*).

Final corrected $\Delta_{47}$ values on the I-CDES scale were averaged per sample, before temperatures were calculated using the combined foraminifera-based calibration of (Meinicke et al., 2020), updated to the I-CDES scale by (Meinicke et al., 2021), that is based on three different calibration datasets measured in two different laboratories:

$$\Delta_{47}(I-CDES) = (0.0397 \pm 0.0011) * \frac{10^6}{T^2} + (0.1518 \pm 0.0128)$$

Thereby, temperature is given in °K. Choosing a different calibration has only a small effect on the results (Fig. S3), as long as calibrations are based on the same carbonate standardization approach. We tested i) the travertine-based calibration of (Kele et al., 2015), as recalculated by (Bernasconi et al., 2018), using $\Delta_{47}$ from our samples standardized to the original values of the ETH standards published by (Bernasconi et al., 2018), and ii) the combined inorganic-biogenic carbonate calibration of (Anderson et al., 2021) covering a temperature range of more than 1000 °C. The differences between temperatures calculated with these equations and our preferred approach are -1.0 to 0.9 °C for (i) and -1.9 °C for (ii). For this study, we chose to use the foraminifera-based calibration (Meinicke et al., 2020), as it contains most foraminifera data, treats these in a consistent way (e.g., calculation of calcification temperatures), and has a larger data density in the interval of ocean temperatures compared to the travertine calibration. It furthermore avoids the influence of analytical uncertainty of sparse measurements on high-temperature samples and possible effects of the $\Delta_{47}$ dependence on temperature deviating from $1/T^2$ over large temperature ranges (Guo et al., 2009).

All temperatures are plotted with 68% and 95% confidence intervals on the average temperatures, which combine the analytical uncertainty and the calibration uncertainty of (Meinicke et al., 2020; their Fig. A2), updated by (Meinicke et al., 2021) using a Monte Carlo approach that samples a random slope-intercept pair for the calibration and a random $\Delta_{47}$ value from their respective probability distributions (5000 iterations). In addition, the number of replicates is indicated by different grey shading in order to optically give more weight to the better replicated analyses. LOESS smoothing was applied to the full North Atlantic temperature data set, taking into account the confidence levels of each data point. Assuming normal distribution of errors, we applied a Monte Carlo method to generate 10,000 realizations of the temperature time series. A LOESS curve (span = 0.2, degree = 1) was then fitted to each of the 10,000 realizations. These LOESS fits served as a basis for calculating 95% confidence intervals (2.5 and 97.5 percentiles; grey shading in Figures 1 and 2).

2. $\delta^{13}C$, $\delta^{18}O$, $\delta^{18}O_{sw}$

$\delta^{13}C$ and $\delta^{18}O$ values were calibrated to the Vienna Pee Dee Belemnite (VPDB) scale with the ETH 1-4 carbonate standards that were also used for $\Delta_{47}$ corrections in a similar moving window approach with standard results from several days. The clumped isotope standards have previously been calibrated to the VPDB scale using the international carbonate standards NBS-18, NBS-19, and LSVEC (Bernasconi et al., 2018). In the case of $\delta^{18}O$, the standard correction also accounted for minor variations in $\delta^{18}O$ scale compression.

$\delta^{18}O_{sw}$ was calculated from the $\Delta_{47}$ temperatures and the $\delta^{18}O_b$ values determined from *Cibicidoides spec.*, using a temperature- $\delta^{18}O_b$ relationship derived for that genus (Marchitto et al., 2014; equation 9). For early Eocene data from Walvis Ridge and Maud Rise, where *Cibicidoides* were not measured, $\delta^{18}O_b$ from *Nuttalides* and *Oridorsalis* were first corrected for inter-species offsets from *Cibicidoides* using the relationships suggested by (Katz et al., 2003).

## 3. Deep Ocean pH

Boron isotope data from benthic foraminifera were generated from the North Atlantic (U1409) and Central Atlantic (ODP 1258 and 1260, 45-52 Ma) and combined with published data from the Central Atlantic (ODP 999 and 926 (Greenop et al., 2017)) – see Table S2 for details. These sites span paleo-depths from 2.5-3.6 km, which are today bathed by northern-sourced waters with similar properties (Rae and Broecker, 2018), and we find consistent values between sites in our record. Analyses were made on mono-specific samples of the genus *Cibicidoides*: *C. wuellerstorfi* and *C. mundulus* in the Neogene and *C. eocaenus*, *C. havanensis*, and *C. velascoensis* in the Paleogene.

**Table S2**. Site information for benthic boron isotope samples with approximate paleo water depths for the respective age intervals

| Site | Present location | Age range of benthic $\delta^{11}B$ data | Paleo water depth (m) |
|---|---|---|---|
| U1409 | 41°17.7'N, 49°14.0°W | 53-59 Ma | 2500 |
| 1258 | 9°26.0'N, 54°44.0°W | 47-52 Ma | 3200 |
| 1260 | 9°16.0'N, 54°33.0°W | 45-46 Ma | 2500 |
| 926 | 3°43.1'N, 42°54.5°W | 5-23 Ma | 3600 |
| 999 | 12°44.6'N, 78°44.4°W | 0-3 Ma | 2800 |

Analytical methods followed established protocols (e.g., Foster et al., 2013; Rae et al., 2018; Rae et al., 2011). In brief, foraminifera were crushed, oxidatively cleaned with hydrogen peroxide, and dissolved following (Rae et al., 2011). A small split (<5 %) of the sample was analyzed for minor and trace element composition by ICPMS to assess boron content and sample cleanliness. Boron was then removed from the sample matrix, using ion exchange column chromatography with

Amberlite 743, and analyzed by MC-ICPMS. Data were obtained from site U1409 in the St Andrews isotope Geochemistry (STAiG) laboratories at the University of St Andrews and from sites 1258 and 1260 in the Bristol Isotope Group (BIG) at the University of Bristol. Analyses in these laboratories follow very similar protocols, though with some minor differences (boron washout assisted using $NH_3$ at BIG, HF at STAiG; and signal detection using $10^{11}$ Ω amplifiers at BIG, $10^{13}$ Ω amplifiers at STAiG). Cross calibration between these laboratories has been ensured by participation in interlaboratory comparison exercises (Foster et al., 2013; Gutjahr et al., 2021; Stewart et al., 2020) and use of identical primary and consistency standards, yielding consistent values (e.g. the pooled 2SD of boric acid consistency standards measured across both laboratories during these analytical sessions is 0.17 ‰, n=8). Uncertainties are reported at 2SD based on long-term reproducibility of samples of this size in each lab.

Calculation of deep ocean pH as shown in Figure 2C follows the procedures in (Rae, 2018) and (Rae et al., 2021). We assume that these epifaunal *Cibicidoides* species record bottom water $\delta^{11}B$ of borate, as seen in modern calibrations (Rae et al., 2011). To calculate the boric acid dissociation constant ($K_B$) we interpolate the smoothed clumped isotope temperature record presented here (Fig. 1A), use salinity of 35, paleo water depths as shown in Table S2 (noting that depth and salinity have little influence on calculated pH), and we account for the (minor) influence of changing seawater $[Ca^{2+}]$ and $[Mg^{2+}]$ (e.g., Brennan et al., 2013) using MyAMI (Hain et al., 2015) as in (Rae et al., 2021). We use the compilation of $\delta^{11}B_{SW}$ estimates from (Rae et al., 2021). The influence of ±0.5 ‰ in $\delta^{11}B_{SW}$ on pH is shown with the shaded area in Figure 2C and the influence of analytical uncertainties in $\delta^{11}B$ and ± 2 °C in temperature are shown by the 2SD error bars, based on the standard deviation of a 10,000 member Monte Carlo ensemble.

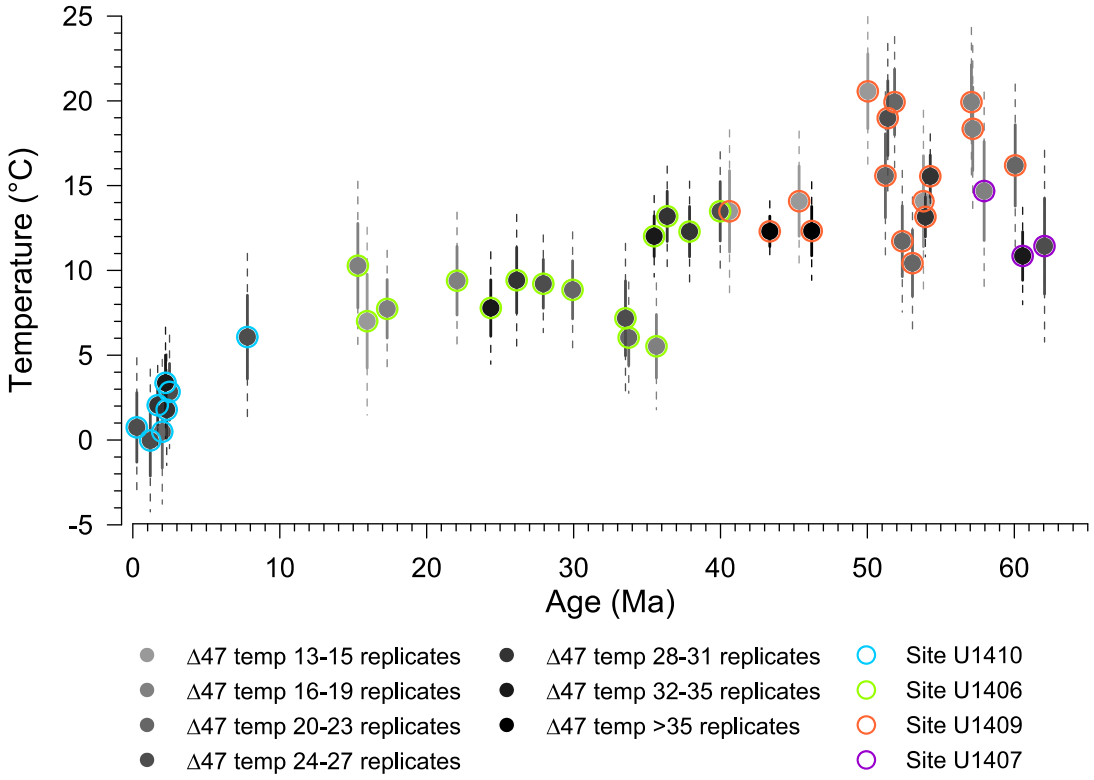


**Fig. S1: North Atlantic IODP Expedition 342 Sites used for the different parts of the record.** Note the close reproducibility of temperatures at 40 Ma, with overlapping data from two sites with very different depths in meters below sea floor (mbsf) in each (1406B core 28 at 268 mbsf vs. 1409C core 5 at 44 mbsf). See also the respective SEM images of foraminifer tests from each of these two samples in Figure S2.

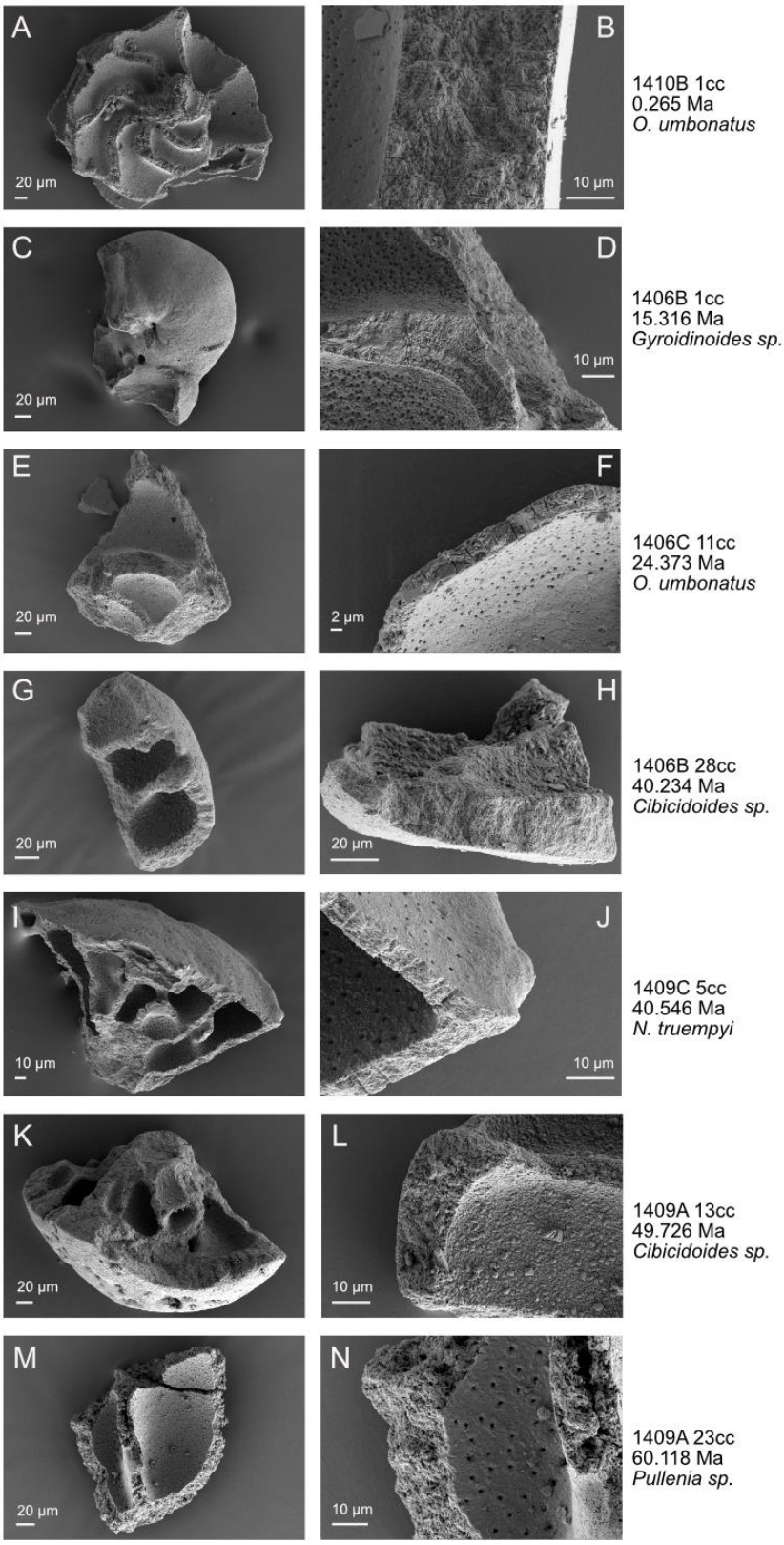


**Fig. S2. SEM images of benthic foraminifera analyzed for clumped isotopes spanning the Cenozoic record.** Preservation state is generally good to excellent (clearly visible microstructures such as pores and layered structure of wall cross-sections), but shows the expected deterioration (addition of blocky calcite overgrowth) with depth (increasing core number X in "Xcc"). Note for example the different extent of overgrowth on two samples for ~40 Ma stemming from different sites and burial depths (G, H vs. I, J). The sample from 1406B 28cc shows blocky calcite overgrowth on the inside of the shell fragment (H), which is not observed on the fragment from 1409C 5cc (J). These samples yielded nonetheless indistinguishable temperatures.

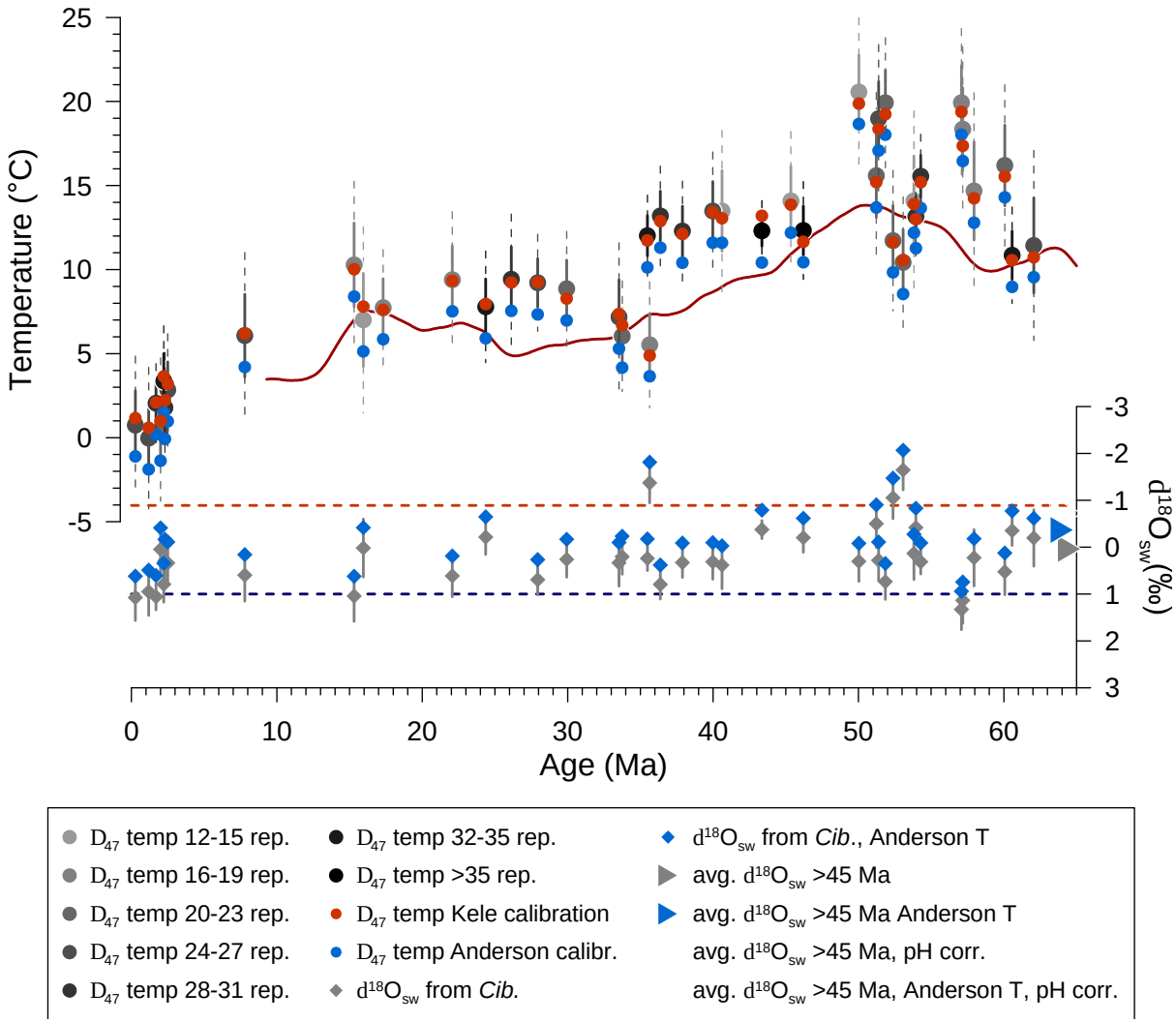


**Fig. S3. Influence of different clumped isotope calibration on reconstructed temperatures and $\delta^{18}O_{sw}$.** The calibration used in this study is based on a compilation of planktic and benthic foraminifera from surface sediments (Meinicke et al., 2020), updated to the I-CDES scale by (Meinicke et al., 2021). The grey symbols in the top and bottom panels represent the North Atlantic data calculated with this calibration and are the same as shown in Figs. 1A and 2A and in Fig. 2D, respectively. The results match well to the temperatures obtained when using a calibration based on travertines and tufas covering a larger temperature range ("Kele calibration" (Kele et al., 2015), recalculated by (Bernasconi et al., 2018)) with differences of -1.0 to 0.9 °C. The differences to this calibration include the effects of slightly different standardization (CDES versus I-CDES scale). A recent calibration covering a temperature range of 1000°C and including previous calibration data including most, but not all, of the above (Anderson et al., 2021), on the other hand yields temperatures slightly colder (by 1.9 °C), but the general observations remain unchanged. With this ("Anderson") calibration, $\delta^{18}O_{sw}$ is 0.4 ‰ heavier (blue symbols in bottom panel). Average $\delta^{18}O_{sw}$ for >45 Ma (arrows to the right) with and without a pH correction become -1.13 ‰ and -0.37 ‰,

respectively. Here we chose to use the foraminifera-based calibration (Meinicke et al., 2020), as it contains most foraminifera data treated in a consistent way and circumvents the analytical uncertainty of few measurements on high-temperature samples influencing the regression (see also methods section).

5

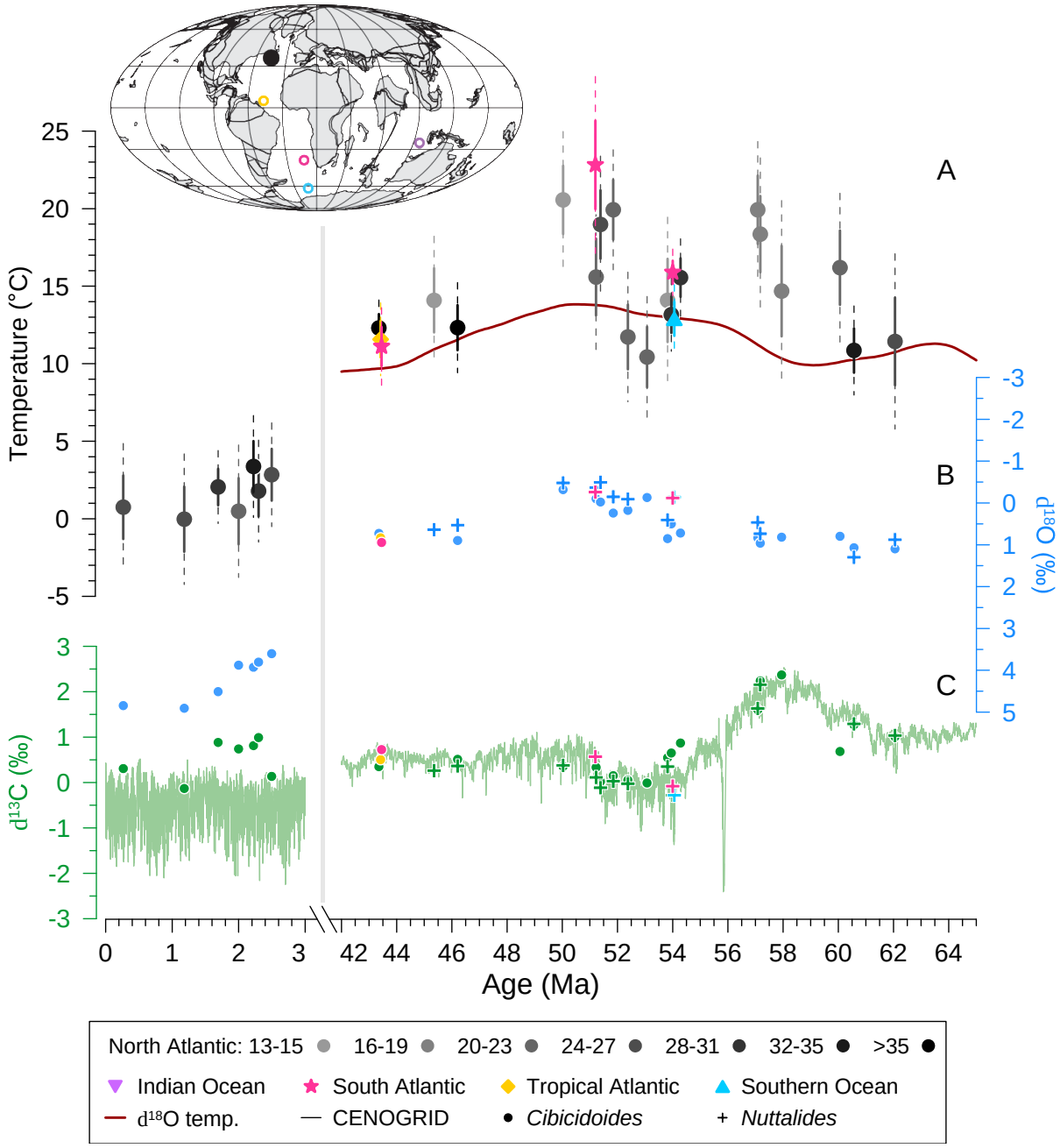


**Fig. S4. Close-up of the early and late Cenozoic intervals of Fig. 1.** As explained in the caption for Fig. 1, some of the apparent offsets in $\delta^{18}O_b$ and $\delta^{13}C$ between our data and CENOGRID are due to adjustments for inter-site/basin offsets in the CENOGRID data set. For example, the South Atlantic data used for most of the Paleocene and early Eocene sections of the CENOGRID record have been adjusted by -0.2 ‰ (Westerhold et al., 2020), but such a correction was not applied to our data for lack of constraints.

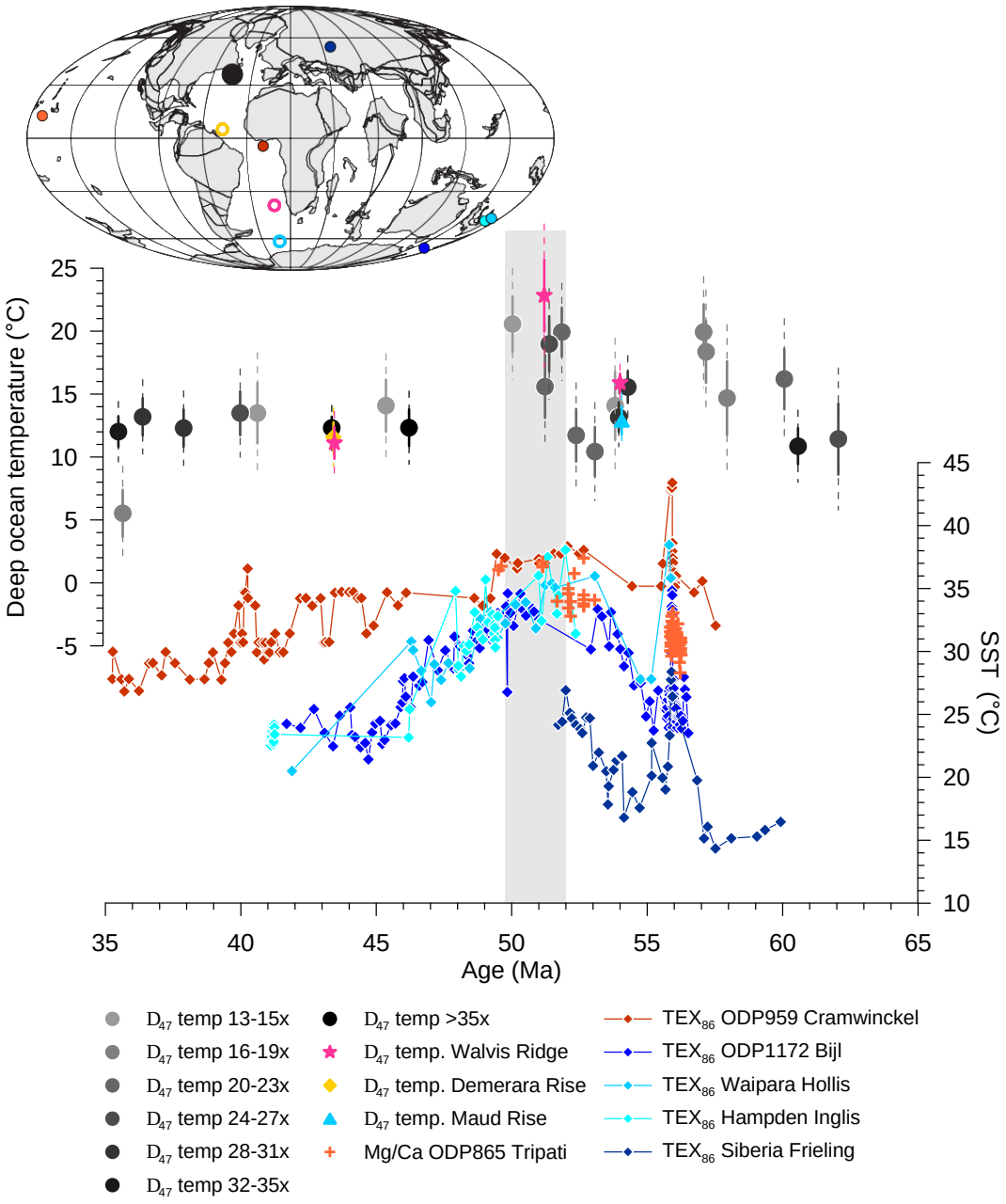


**Fig. S5. Comparison of deep ocean temperatures for the early Cenozoic with the most detailed sea surface temperature (SST) records currently available.** Most SST records that span a significant time period in the Early Cenozoic with sufficient resolution are based on organic biomarkers ($TEX_{86}$ proxy). The SST data shown here (Bijl et al., 2009; Bijl et al., 2013; Cramwinckel et al., 2018; Frieling et al., 2014; Frieling et al., 2018; Hollis et al., 2012; Sluijs et al., 2011; Tripati et al., 2003) were obtained from a recent compilation of early Cenozoic temperature data (Hollis et al., 2019) and age models were updated to the CENOGRID timescale for direct comparison to our data. The grey bar highlights the early Eocene interval of elevated

Atlantic deep ocean temperatures. The locations of the SST sites are indicated on the inset map by closed small circles.

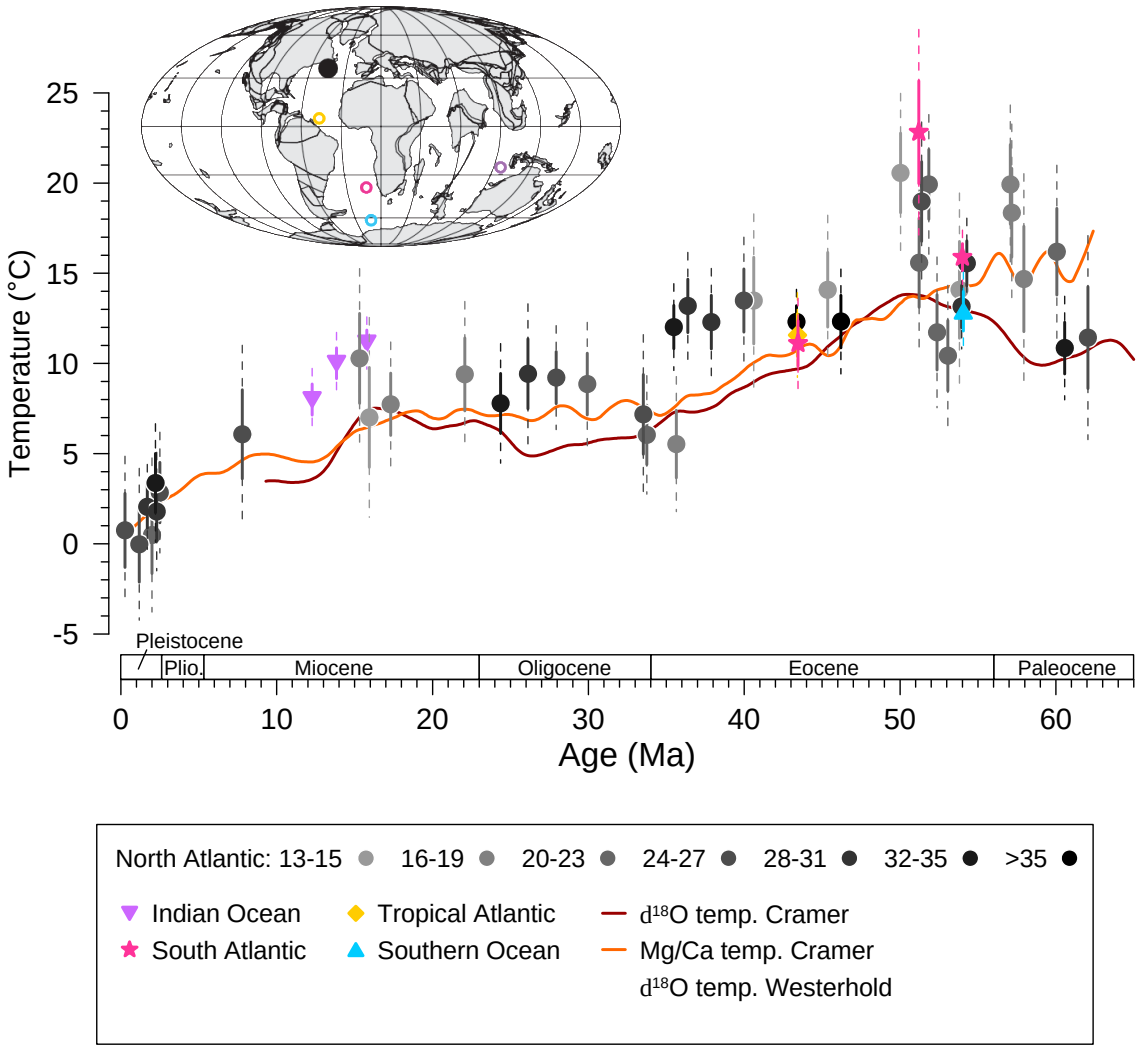


**Fig. S6. Comparison of clumped isotope temperatures to estimates of deep ocean temperature based on $\delta^{18}O$ and Mg/Ca.** Red line with uncertainty band: temperature estimate based on $\delta^{18}O_b$ and reconstructed sea level (Cramer et al., 2011); Orange line: Mg/Ca-based temperature record (*6)*, in the version using Equation 7b of (Cramer et al., 2011) for temperature calculation. This reconstruction is based on a global compilation of selected Mg/Ca records, but in the Paleocene to middle Eocene is based on sparse data predominantly from the Pacific Ocean. Light blue line: CENOGRID $\delta^{18}O_b$ -based deep ocean temperature (Westerhold et al., 2020) calculated with the approach suggested by Hansen (Hansen et al., 2013), which accounts for the varying contribution of ice sheet size by defining three different equations for different time intervals (0-3.6 Ma, 3.6-34 Ma, and prior to 34 Ma). Grey and colored symbols: Clumped isotope temperatures with uncertainties as in Figs. 1 and 2. Previous estimates are plotted on their published age models.

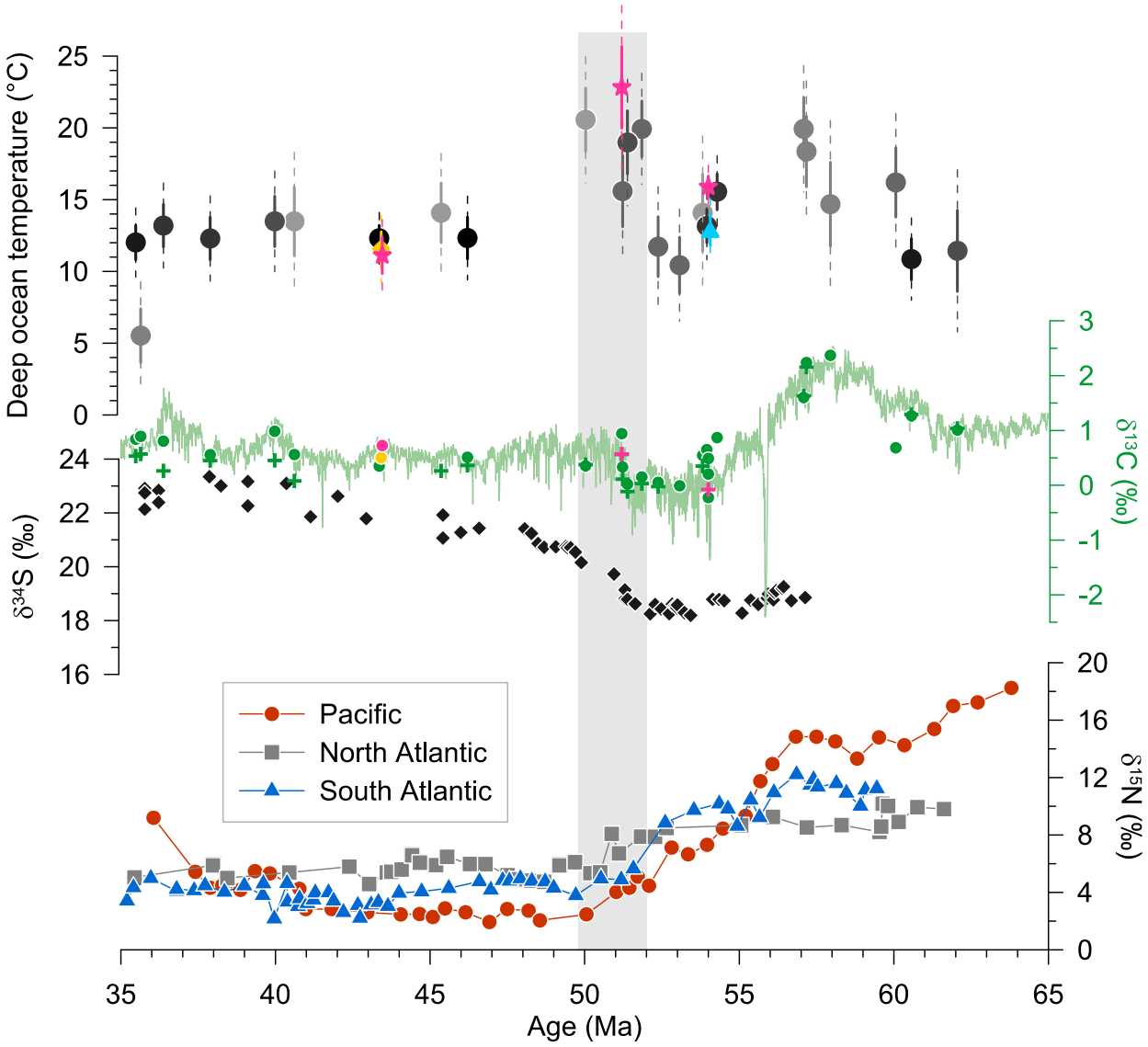


**Figure S7. Comparison of the deep ocean temperatures to proxy records of biogeochemical cycles for the Palocene-Eocene.** $\delta^{13}C$ data are as in Fig. 1C, $\delta^{34}S$ data are from multiple sites (Rennie et al., 2018), and $\delta^{15}N$ data are from three different sites (Kast et al., 2019) as indicated in the legend.

**Data S1. (separate file)**

Isotope data averaged per sample

**Data S2. (separate file)**

Numbers of $\Delta_{47}$ aliquots analyzed per species/genus for each sample

**References and Notes**

Agterhuis, T., Ziegler, M. and Lourens, L. (in revision) Extreme deep-sea warmth supports high climate sensitivity in the early Eocene hothouse.

Anagnostou, E., John, E.H., Babila, T.L., Sexton, P.F., Ridgwell, A., Lunt, D.J., Pearson, P.N., Chalk, T.B., Pancost, R.D. and Foster, G.L. (2020) Proxy evidence for state-dependence of climate sensitivity in the Eocene greenhouse. Nat Commun 11, 4436.

Anderson, N.T., Kelson, J.R., Kele, S., Daeron, M., Bonifacie, M., Horita, J., Mackey, T.J., John, C.M., Kluge, T., Petschnig, P., Jost, A.B., Huntington, K.W., Bernasconi, S.M. and Bergmann, K.D. (2021) A Unified Clumped Isotope Thermometer Calibration (0.5-1,100 degrees C) Using Carbonate-Based Standardization. Geophys. Res. Lett. 48.

Bernard, S., Daval, D., Ackerer, P., Pont, S. and Meibom, A. (2017) Burial-induced oxygen-isotope re-equilibration of fossil foraminifera explains ocean paleotemperature paradoxes. Nat Commun 8, 1134.

Bernasconi, S.M., Daëron, M., Bergmann, K.D., Bonifacie, M., Meckler, A.N., Affek, H.P., Anderson, N., Bajnai, D., Barkan, E., Beverly, E., Blamart, D., Burgener, L., Calmels, D., Chaduteau, C., Clog, M., Davidheiser-Kroll, B., Davies, A., Dux, F., Eiler, J., Elliott, B., Fetrow, A.C., Fiebig, J., Goldberg, S., Hermoso, M., Huntington, K.W., Hyland, E., Ingalls, M., Jaggi, M., John, C.M., Jost, A.B., Katz, S., Kelson, J., Kluge, T., Kocken, I.J., Laskar, A., Leutert, T.J., Liang, D., Lucarelli, J., Mackey, T.J., Mangenot, X., Meinicke, N., Modestou, S.E., Müller, I.A., Murray, S., Neary, A., Packard, N., Passey, B.H., Pelletier, E., Petersen, S., Piasecki, A., Schauer, A., Snell, K.E., Swart, P.K., Tripati, A., Upadhyay, D., Vennemann, T., Winkelstern, I., Yarian, D., Yoshida, N., Zhang, N. and Ziegler, M. (2021) InterCarb: A Community Effort to Improve Interlaboratory Standardization of the Carbonate Clumped Isotope Thermometer Using Carbonate Standards. Geochemistry, Geophysics, Geosystems 22, e2020GC009588.

Bernasconi, S.M., Muller, I.A., Bergmann, K.D., Breitenbach, S.F.M., Fernandez, A., Hodell, D.A., Jaggi, M., Meckler, A.N., Millan, I. and Ziegler, M. (2018) Reducing Uncertainties in Carbonate Clumped Isotope Analysis Through Consistent Carbonate-Based Standardization. Geochem Geophy Geosy 19, 2895-2914.

Bijl, P.K., Schouten, S., Sluijs, A., Reichart, G.J., Zachos, J.C. and Brinkhuis, H. (2009) Early Palaeogene temperature evolution of the southwest Pacific Ocean. Nature 461, 776-779.

Bijl, P.K., Sluijs, A. and Brinkhuis, H. (2013) A magneto- and chemostratigraphically calibrated dinoflagellate cyst zonation of the early Palaeogene South Pacific Ocean. Earth-Sci. Rev. 124, 1-31.

Brennan, S.T., Lowenstein, T.K. and Cendon, D.I. (2013) The Major-Ion Composition of Cenozoic Seawater: The Past 36 Million Years from Fluid Inclusions in Marine Halite. Am J Sci 313, 713-775.

Burke, K.D., Williams, J.W., Chandler, M.A., Haywood, A.M., Lunt, D.J. and Otto-Bliesner, B.L. (2018) Pliocene and Eocene provide best analogs for near-future climates. Proc. Natl. Acad. Sci. U. S. A. 115, 13288-13293.

Cramer, B.S., Miller, K.G., Barrett, P.J. and Wright, J.D. (2011) Late Cretaceous-Neogene trends in deep ocean temperature and continental ice volume: Reconciling records of benthic foraminiferal geochemistry (delta O-18 and Mg/Ca) with sea level history. J. Geophys. Res.-Oceans 116, C12023.

Cramwinckel, M.J., Huber, M., Kocken, I.J., Agnini, C., Bijl, P.K., Bohaty, S.M., Frieling, J., Goldner, A., Hilgen, F.J., Kip, E.L., Peterse, F., van der Ploeg, R., Rohl, U., Schouten, S. and Sluijs, A. (2018) Synchronous tropical and polar temperature evolution in the Eocene. Nature 559, 382-+.

Davies, A., Greselle, B., Hunter, S.J., Baines, G., Robson, C., Haywood, A.M., Ray, D.C., Simmons, M.D. and van Buchem, F.S.P. (2020) Assessing the impact of aquifer-eustasy on short-term Cretaceous sea-level. Cretaceous Res 112, 104445.

Douglas, P.M.J., Affek, H.P., Ivany, L.C., Houben, A.J.P., Sijp, W.P., Sluijs, A., Schouten, S. and Pagani, M. (2014) Pronounced zonal heterogeneity in Eocene southern high-latitude sea surface temperatures. Proc. Natl. Acad. Sci. U. S. A. 111, 6582-6587.

Eiler, J.M. (2007) "Clumped-isotope" geochemistry - The study of naturally-occurring, multiply-substituted isotopologues. Earth Planet. Sci. Lett. 262, 309-327.

Evans, D., Badger, M.P.S., Foster, G.L., Henehan, M.J., Lear, C.H. and Zachos, J.C. (2018) No substantial long-term bias in the Cenozoic benthic foraminifera oxygen-isotope record. Nat Commun 9.

Foster, G.L., Honisch, B., Paris, G., Dwyer, G.S., Rae, J.W.B., Elliott, T., Gaillardet, J., Hemming, N.G., Louvat, P. and Vengosh, A. (2013) Interlaboratory comparison of boron isotope analyses of boric acid, seawater and marine CaCO3 by MC-ICPMS and NTIMS. Chem Geol 358, 1-14.

Frieling, J., Iakovleva, A.I., Reichart, G.J., Aleksandrova, G.N., Gnibidenko, Z.N., Schouten, S. and Sluijs, A. (2014) Paleocene-Eocene warming and biotic response in the epicontinental West Siberian Sea. Geology 42, 767-770.

Frieling, J., Reichart, G.J., Middelburg, J.J., Rohl, U., Westerhold, T., Bohaty, S.M. and Sluijs, A. (2018) Tropical Atlantic climate and ecosystem regime shifts during the Paleocene-Eocene Thermal Maximum. Clim Past 14, 39-55.

Gaina, C. and Jakob, J. (2019) Global Eocene tectonic unrest: Possible causes and effects around the North American plate. Tectonophysics 760, 136-151.

Grauel, A.L., Schmid, T.W., Hu, B., Bergami, C., Capotondi, L., Zhou, L.P. and Bernasconi, S.M. (2013) Calibration and application of the 'clumped isotope' thermometer to foraminifera for high-resolution climate reconstructions. Geochim. Cosmochim. Acta 108, 125-140.

Greenop, R., Hain, M.P., Sosdian, S.M., Oliver, K.I.C., Goodwin, P., Chalk, T.B., Lear, C.H., Wilson, P.A. and Foster, G.L. (2017) A record of Neogene seawater delta B-11 reconstructed from paired delta B-11 analyses on benthic and planktic foraminifera. Clim Past 13, 149-170.

Guo, W.F. (2020) Kinetic clumped isotope fractionation in the DIC-H2O-CO2 system: Patterns, controls, and implications. Geochim. Cosmochim. Acta 268, 230-257.

Guo, W.F., Mosenfelder, J.L., Goddard, W.A. and Eiler, J.M. (2009) Isotopic fractionations associated with phosphoric acid digestion of carbonate minerals: Insights from first-principles theoretical modeling and clumped isotope measurements. Geochim. Cosmochim. Acta 73, 7203-7225.

Gutjahr, M., Bordier, L., Douville, E., Farmer, J., Foster, G.L., Hathorne, E.C., Honisch, B., Lemarchand, D., Louvat, P., McCulloch, M., Noireaux, J., Pallavicini, N., Rae, J.W.B., Rodushkin, I., Roux, P., Stewart, J.A., Thil, F. and You, C.F. (2021) Sub-Permil Interlaboratory Consistency for Solution-Based Boron Isotope Analyses on Marine Carbonates. Geostand Geoanal Res 45, 59-75.

Hain, M.P., Sigman, D.M., Higgins, J.A. and Haug, G.H. (2015) The effects of secular calcium and magnesium concentration changes on the thermodynamics of seawater acid/base chemistry: Implications for Eocene and Cretaceous ocean carbon chemistry and buffering. Glob. Biogeochem. Cycle 29, 517-533.

Hansen, J., Sato, M., Russell, G. and Kharecha, P. (2013) Climate sensitivity, sea level and atmospheric carbon dioxide. Philos T R Soc A 371, 20120294.

Hollis, C.J., Jones, T.D., Anagnostou, E., Bijl, P.K., Cramwinckel, M.J., Cui, Y., Dickens, G.R., Edgar, K.M., Eley, Y., Evans, D., Foster, G.L., Frieling, J., Inglis, G.N., Kennedy, E.M., Kozdon, R., Lauretano, V., Lear, C.H., Littler, K., Lourens, L., Meckler, A.N., Naafs, B.D.A., Palike, H., Pancost, R.D., Pearson, P.N., Rohl, U., Royer, D.L., Salzmann, U., Schubert, B.A., Seebeck, H., Sluijs, A., Speijer, R.P., Stassen, P., Tierney, J., Tripati, A., Wade, B., Westerhold, T., Witkowski, C., Zachos, J.C., Zhang, Y.G., Huber, M. and Lunt, D.J. (2019) The DeepMIP contribution to PMIP4: methodologies for selection, compilation and analysis of latest Paleocene and early Eocene climate proxy data, incorporating version 0.1 of the DeepMIP database. Geosci Model Dev 12, 3149-3206.

Hollis, C.J., Taylor, K.W.R., Handley, L., Pancost, R.D., Huber, M., Creech, J.B., Hines, B.R., Crouch, E.M., Morgans, H.E.G., Crampton, J.S., Gibbs, S., Pearson, P.N. and Zachos, J.C. (2012) Early Paleogene temperature history of the Southwest Pacific Ocean: Reconciling proxies and models. Earth Planet. Sci. Lett. 349, 53-66.

Hu, B., Radke, J., Schluter, H.J., Heine, F.T., Zhou, L.P. and Bernasconi, S.M. (2014) A modified procedure for gas-source isotope ratio mass spectrometry: the long-integration dual-inlet (LIDI) methodology and implications for clumped isotope measurements. Rapid Commun Mass Sp 28, 1413-1425.

Inglis, G.N., Bragg, F., Burls, N.J., Cramwinckel, M.J., Evans, D., Foster, G.L., Huber, M., Lunt, D.J., Siler, N., Steinig, S., Tierney, J.E., Wilkinson, R., Anagnostou, E., de Boer, A.M., Jones, T.D., Edgar, K.M., Hollis, C.J., Hutchinson, D.K. and Pancost, R.D. (2020) Global mean surface temperature and climate sensitivity of the early Eocene Climatic Optimum (EECO), Paleocene-Eocene Thermal Maximum (PETM), and latest Paleocene. Clim Past 16, 1953-1968.

John, C.M. and Bowen, D. (2016) Community software for challenging isotope analysis: First applications of "Easotope' to clumped isotopes. Rapid Communications in Mass Spectrometry 30, 2285-2300.

Kast, E.R., Stolper, D.A., Auderset, A., Higgins, J.A., Ren, H.J., Wang, X.C.T., Martinez-Garcia, A., Haug, G.H. and Sigman, D.M. (2019) Nitrogen isotope evidence for expanded ocean suboxia in the early Cenozoic. Science 364, 386-389.

Katz, M.E., Katz, D.R., Wright, J.D., Miller, K.G., Pak, D.K., Shackleton, N.J. and Thomas, E. (2003) Early Cenozoic benthic foraminiferal isotopes: Species reliability and interspecies correction factors. Paleoceanography 18, 1024.

Kele, S., Breitenbach, S.F.M., Capezzuoli, E., Meckler, A.N., Ziegler, M., Millan, I.M., Kluge, T., Deak, J., Hanselmann, K., John, C.M., Yan, H., Liu, Z.H. and Bernasconi, S.M. (2015) Temperature dependence of oxygen- and clumped isotope fractionation in carbonates: A study of travertines and tufas in the 6-95 degrees C temperature range. Geochim. Cosmochim. Acta 168, 172-192.

Lear, C.H., Elderfield, H. and Wilson, P.A. (2000) Cenozoic deep-sea temperatures and global ice volumes from Mg/Ca in benthic foraminiferal calcite. Science 287, 269-272.

Leutert, T.J., Modestou, S., Bernasconi, S.M. and Meckler, A.N. (2021) Southern Ocean bottom-water cooling and ice sheet expansion during the middle Miocene climate transition. Clim. Past 17, 2255-2271.

Leutert, T.J., Sexton, P.F., Tripati, A., Piasecki, A., Ho, S.L. and Meckler, A.N. (2019) Sensitivity of clumped isotope temperatures in fossil benthic and planktic foraminifera to diagenetic alteration. Geochim. Cosmochim. Acta 257, 354-372.

Liebrand, D., de Bakker, A.T.M., Beddow, H.M., Wilson, P.A., Bohaty, S.M., Ruessink, G., Palike, H., Batenburg, S.J., Hilgen, F.J., Hodell, D.A., Huck, C.E., Kroon, D., Raffi, I., Saes,

M.J.M., van Dijk, A.E. and Lourens, L.J. (2017) Evolution of the early Antarctic ice ages. Proc. Natl. Acad. Sci. U. S. A. 114, 3867-3872.

Lunt, D.J., Bragg, F., Chan, W.L., Hutchinson, D.K., Ladant, J.B., Morozova, P., Niezgodzki, I., Steinig, S., Zhang, Z.S., Zhu, J., Abe-Ouchi, A., Anagnostou, E., de Boer, A.M., Coxall, H.K., Donnadieu, Y., Foster, G., Inglis, G.N., Knorr, G., Langebroek, P.M., Lear, C.H., Lohmann, G., Poulsen, C.J., Sepulchre, P., Tierney, J.E., Valdes, P.J., Volodin, E.M., Jones, T.D., Hollis, C.J., Huber, M. and Otto-Bliesner, B.L. (2021) DeepMIP: model intercomparison of early Eocene climatic optimum (EECO) large-scale climate features and comparison with proxy data. Clim Past 17, 203-227.

Marchitto, T.M., Curry, W.B., Lynch-Stieglitz, J., Bryan, S.P., Cobb, K.M. and Lund, D.C. (2014) Improved oxygen isotope temperature calibrations for cosmopolitan benthic foraminifera. Geochim. Cosmochim. Acta 130, 1-11.

Meckler, A.N., Ziegler, M., Millán, M.I., Breitenbach, S.F.M. and Bernasconi, S.M. (2014) Long-term performance of the Kiel carbonate device with a new correction scheme for clumped isotope measurements. Rapid Commun. Mass Spectrom. 28, 1705-1715.

Meinicke, N., Ho, S.L., Hannisdal, B., Nurnberg, D., Tripati, A., Schiebel, R. and Meckler, A.N. (2020) A robust calibration of the clumped isotopes to temperature relationship for foraminifers. Geochim. Cosmochim. Acta 270, 160-183.

Meinicke, N., Reimi, M.A., Ravelo, A.C. and Meckler, A.N. (2021) Coupled Mg/Ca and clumped isotope measurements confirm lack of substantial mixed layer cooling in the Western Pacific warm pool over the last 5 million years. Paleoceanogr Paleocl 36, e2020PA004115.

Modestou, S.E., Leutert, T.J., Fernandez, A., Lear, C.H. and Meckler, A.N. (2020) Warm Middle Miocene Indian Ocean Bottom Water Temperatures: Comparison of Clumped Isotope and Mg/Ca-Based Estimates. Paleoceanogr Paleocl 35, e2020PA003927.

Muller, R.D., Sdrolias, M., Gaina, C., Steinberger, B. and Heine, C. (2008) Long-term sea-level fluctuations driven by ocean basin dynamics. Science 319, 1357-1362.

Peral, M., Daeron, M., Blamart, D., Bassinot, F., Dewilde, F., Smialkowski, N., Isguder, G., Bonnin, J., Jorissen, F., Kissel, C., Michel, E., Riveiros, N.V. and Waelbroeck, C. (2018) Updated calibration of the clumped isotope thermometer in planktonic and benthic foraminifera. Geochim. Cosmochim. Acta 239, 1-16.

Piasecki, A., Bernasconi, S.M., Grauel, A.L., Hannisdal, B., Ho, S.L., Leutert, T.J., Marchitto, T.M., Meinicke, N., Tisserand, A. and Meckler, N. (2019) Application of Clumped Isotope Thermometry to Benthic Foraminifera. Geochem Geophy Geosy 20, 2082-2090.

Rae, J.W.B. (2018) Boron Isotopes in Foraminifera: Systematics, Biomineralisation, and CO2 Reconstruction, in: Marschall, H., Foster, G. (Eds.), Boron Isotopes. The Fifth Element. Springer, pp. 107-143.

Rae, J.W.B. and Broecker, W. (2018) What fraction of the Pacific and Indian oceans' deep water is formed in the Southern Ocean? Biogeosciences 15, 3779-3794.

Rae, J.W.B., Burke, A., Robinson, L.F., Adkins, J.F., Chen, T., Cole, C., Greenop, R., Li, T., Littley, E.F.M., Nita, D.C., Stewart, J.A. and Taylor, B.J. (2018) CO2 storage and release in the deep Southern Ocean on millennial to centennial timescales. Nature 562, 569-573.

Rae, J.W.B., Foster, G.L., Schmidt, D.N. and Elliott, T. (2011) Boron isotopes and B/Ca in benthic foraminifera: Proxies for the deep ocean carbonate system. Earth Planet. Sci. Lett. 302, 403-413.

Rae, J.W.B., Zhang, Y.G., Liu, X., Foster, G.L., Stoll, H.M. and Whiteford, R.D.M. (2021) Atmospheric CO2 over the Past 66 Million Years from Marine Archives. Annu Rev Earth Pl Sc, 609-641.

Rennie, V.C.F., Paris, G., Sessions, A.L., Abramovich, S., Turchyn, A.V. and Adkins, J.F. (2018) Cenozoic record of delta S-34 in foraminiferal calcite implies an early Eocene shift to deep-ocean sulfide burial. Nature Geoscience 11, 761-765.

Scientists, E. (2012) Paleogene Newfoundland sediment drifts. IODP Preliminary Report 342.

Sliwinska, K.K., Thomsen, E., Schouten, S., Schoon, P.L. and Heilmann-Clausen, C. (2019) Climate- and gateway-driven cooling of Late Eocene to earliest Oligocene sea surface temperatures in the North Sea Basin. Sci Rep-Uk 9, 4458.

Sluijs, A., Bijl, P.K., Schouten, S., Rohl, U., Reichart, G.J. and Brinkhuis, H. (2011) Southern ocean warming, sea level and hydrological change during the Paleocene-Eocene thermal maximum. Clim Past 7, 47-61.

Spero, H.J., Bijma, J., Lea, D.W. and Bemis, B.E. (1997) Effect of seawater carbonate concentration on foraminiferal carbon and oxygen isotopes. Nature 390, 497-500.

Stewart, J.A., Robinson, L.F., Day, R.D., Strawson, I., Burke, A., Rae, J.W.B., Spooner, P.T., Samperiz, A., Etnoyer, P.J., Williams, B., Paytan, A., Leng, M.J., Haussermann, V., Wickes, L.N., Bratt, R. and Pryer, H. (2020) Refining trace metal temperature proxies in cold-water scleractinian and stylasterid corals. Earth Planet. Sci. Lett. 545, 116412.

Stolper, D.A., Eiler, J.M. and Higgins, J.A. (2018) Modeling the effects of diagenesis on carbonate clumped-isotope values in deep- and shallow-water settings. Geochim. Cosmochim. Acta 227, 264-291.

Tang, J.W., Dietzel, M., Fernandez, A., Tripati, A.K. and Rosenheim, B.E. (2014) Evaluation of kinetic effects on clumped isotope fractionation (Delta(47)) during inorganic calcite precipitation. Geochim. Cosmochim. Acta 134, 120-136.

Thiagarajan, N., Subhas, A.V., Southon, J.R., Eiler, J.M. and Adkins, J.F. (2014) Abrupt pre-Bolling-Allerod warming and circulation changes in the deep ocean. Nature 511, 75-78.

Tripati, A., Backman, J., Elderfield, H. and Ferretti, P. (2005) Eocene bipolar glaciation associated with global carbon cycle changes. Nature 436, 341-346.

Tripati, A. and Elderfield, H. (2005) Deep-sea temperature and circulation changes at the Paleocene-Eocene thermal maximum. Science 308, 1894-1898.

Tripati, A.K., Delaney, M.L., Zachos, J.C., Anderson, L.D., Kelly, D.C. and Elderfield, H. (2003) Tropical sea-surface temperature reconstruction for the early Paleogene using Mg/Ca ratios of planktonic foraminifera. Paleoceanography 18.

Tripati, A.K., Eagle, R.A., Thiagarajan, N., Gagnon, A.C., Bauch, H., Halloran, P.R. and Eiler, J.M. (2010) C-13-O-18 isotope signatures and 'clumped isotope' thermometry in foraminifera and coccoliths. Geochim. Cosmochim. Acta 74, 5697-5717.

Tripati, A.K., Hill, P.S., Eagle, R.A., Mosenfelder, J.L., Tang, J.W., Schauble, E.A., Eiler, J.M., Zeebe, R.E., Uchikawa, J., Coplen, T.B., Ries, J.B. and Henry, D. (2015) Beyond temperature: Clumped isotope signatures in dissolved inorganic carbon species and the influence of solution chemistry on carbonate mineral composition. Geochim. Cosmochim. Acta 166, 344-371.

Tucholke, B.E. and Vogt, P.R. (1979) Western North Atlantic: sedimentary evolution and aspects of tectonic history, in: Tucholke, B., Vogt, P.R. (Eds.), Initial Reports DSDP. U.S. Govt. Printing Office, Washington, DC, pp. 791-825.

Wendler, J.E., Wendler, I., Vogt, C. and Kuss, J. (2016) Link between cyclic eustatic sea-level change and continental weathering: Evidence for aquifer-eustasy in the Cretaceous. Paleogeogr. Paleoclimatol. Paleoecol. 441, 430-437.

Westerhold, T., Marwan, N., Drury, A.J., Liebrand, D., Agnini, C., Anagnostou, E., Barnet, J.S.K., Bohaty, S.M., De Vleeschouwer, D., Florindo, F., Frederichs, T., Hodell, D.A., Holbourn, A.E., Kroon, D., Lauretano, V., Littler, K., Lourens, L.J., Lyle, M., Palike, H., Rohl, U., Tian, J., Wilkens, R.H., Wilson, P.A. and Zachos, J.C. (2020) An astronomically dated record of Earth's climate and its predictability over the last 66 million years. Science 369, 1383-1387.

Zachos, J., Pagani, M., Sloan, L., Thomas, E. and Billups, K. (2001) Trends, rhythms, and aberrations in global climate 65 Ma to present. Science 292, 686-693.

Zeebe, R.E. (2001) Seawater pH and isotopic paleotemperatures of Cretaceous oceans. Paleogeogr. Paleoclimatol. Paleoecol. 170, 49-57.

Zhu, J., Poulsen, C.J., Otto-Bliesner, B.L., Liu, Z.Y., Brady, E.C. and Noone, D.C. (2020) Simulation of early Eocene water isotopes using an Earth system model and its implication for past climate reconstruction. Earth Planet. Sci. Lett. 537.